Available online at www.sciencedirect.com
SCIENCE DIRECT
Catalysis Today 116 (2006) 69–73
CATALYSIS TODAY
www.elsevier.com/locate/cattod

Synthesis and characterization of tungsten and tungsten oxide nanostructured films

F. Di Fonzo, A. Bailini, V. Russo, A. Baserga, D. Cattaneo, M.G. Beghi, P.M. Ossi, C.S. Casari *, A. Li Bassi, C.E. Bottani

NEMAS-Center for NanoEngineered MAterials and Surfaces, Dipartimento di Ingegneria Nucleare, Politecnico di Milano, Via Ponzio 34/3 I-20133 Milano, Italy

Received 13 January 2006; received in revised form 9 February 2006; accepted 10 February 2006
Available online 27 April 2006

Abstract

Nanostructured tungsten and tungsten oxide films have been synthesized by pulsed laser deposition (PLD) in different atmospheres (He, Ar, dry air). The control of the gas pressure in the deposition chamber allows to vary the morphology of the deposited films (studied by scanning electron microscopy (SEM) and atomic force microscopy (AFM)) ranging from a compact ultrasmooth structure to a porous nano and mesostructure characterized by a high fraction of voids and by a large specific area. The presence, the structure and the degree of crystallinity of tungsten oxide have been investigated by Raman spectroscopy. By varying the pressure of the background inert gas (He, Ar) in the 1–1000 Pa range we obtain metallic films with different degrees of spontaneous oxidation when exposed to the atmosphere. Deposition in dry air permits to grow nanostructured tungsten oxide films characterized by different degrees of crystallinity, ranging from amorphous to nanocrystalline.

Keywords: Pulsed laser deposition; Tungsten; Tungsten oxide; Nanostructured thin films

1. Introduction

Tungsten and tungsten oxide films are interesting materials for novel technological applications. Properties of tungsten and tungsten oxide thin films have been explored for electrical contacts in microelectronics [1,2] and for the development of sensors and functional coatings (e.g. smart windows) [3–6]. Increasing interest is devoted to tungsten and tungsten oxide for catalytic applications such as methanol oxidation for fuel cells [7,8], selective oxidation of organic compounds [9], hydrodesulfurization of fuels [10] and isomerization reactions [11,12]. The capability to synthesize bulk materials, films and surfaces with controlled nano and mesostructure opens up the way to tailor the physical (e.g. effective surface area, energy gap) and chemical (e.g. surface reactivity, stoichiometry) properties in view of device development. In this context, the increase of the specific effective surface and the comprehension and control of the electric and optical properties of tungsten oxide coatings is of great importance for the development of the mentioned applications.

Pulsed laser deposition (PLD) is a versatile technique for the synthesis of a wide range of materials [13,14]. The control of the ablation plasma expansion permits to vary the dynamics of the ablated species (atoms, ions and clusters) during their flight before deposition on the substrate. Plume expansion is affected by a background gas in the deposition chamber [15,16]. Provided the pressure is high enough, a background gas increases the collision rate thus favoring cluster formation in the plume [17]. Moreover, clusters loose energy in collisions impinging onto the substrate with a reduced kinetic energy after diffusing in the background atmosphere [18]. PLD in air and N_2 at atmospheric pressure has been already exploited to produce tungsten nanoparticles [19]; some works have been recently devoted to the PLD deposition of tungsten oxide nanostructured films [20,21]. In these cases deposition parameters have been explored and experiments were mainly focused on the optimization of a specific property (i.e. gas sensing and electrochromism).

We report on the capability to grow tungsten and tungsten oxide films with different and controlled nano and mesostructure, ranging from compact to highly porous, by varying the

* Corresponding author.
E-mail address: carlo.casari@polimi.it (C.S. Casari).

0920-5861/$ – see front matter © 2006 Elsevier B.V. All rights reserved.
doi:10.1016/j.cattod.2006.02.080

pressure of a background gas in the 1–1000 Pa range. Pressure and gas type (inert or reactive) influence also the oxidation pathway and the structure of tungsten oxide films.

2. Experimental details

W and WO_3 films have been grown by PLD on silicon substrates at room temperature. UV laser pulses in the nanosecond regime (10–15 ns), from a KrF excimer laser (248 nm wavelength), were focused on a W target (purity 99.99%) with an energy density of roughly 4.5 J/cm^2. This value was chosen in order to maximize deposition rate while minimizing droplet ejection from the target. Films were grown performing 4500 laser pulses at 10 Hz repetition rate (deposition time 7.5 min), with target-to-substrate distance fixed at 50 mm. The deposition rates vary in the 0.2–2 Å/s range moving from deposition in vacuum to 100 Pa He. The UHV compatible deposition chamber is equipped with a 500 l/s turbomolecular pump backed up by a scroll dry pump. The system is equipped with a gas inlet system, a mass flow controller and a full range pressure gauge, thus allowing pressure control over the 10^{-7} Pa to atmospheric range.

SEM micrographs were acquired with a Cambridge Stereoscan using 30 keV primary acceleration voltage and 10 pA probe current. High-resolution images were acquired with a cold field emission Hitachi S-4800 scanning electron microscope. Atomic force microscopy (AFM) measurements were performed with a Thermomicroscope CP Research in non-contact mode with high resonance frequency silicon cantilevers. The film surface root mean square (rms) roughness was estimated from the surface height $z(x, y)$ data measured by AFM. Micro-Raman measurements were performed with a Renishaw InVia spectrometer using the 514.5 nm wavelength of an Ar^+ laser. Spectra were acquired by a 1800 greeds/mm grating, a super-notch filter (cut-off at 100 cm^{-1}) and a Peltier-cooled CCD camera, allowing a spectral resolution of about 3 cm^{-1}.

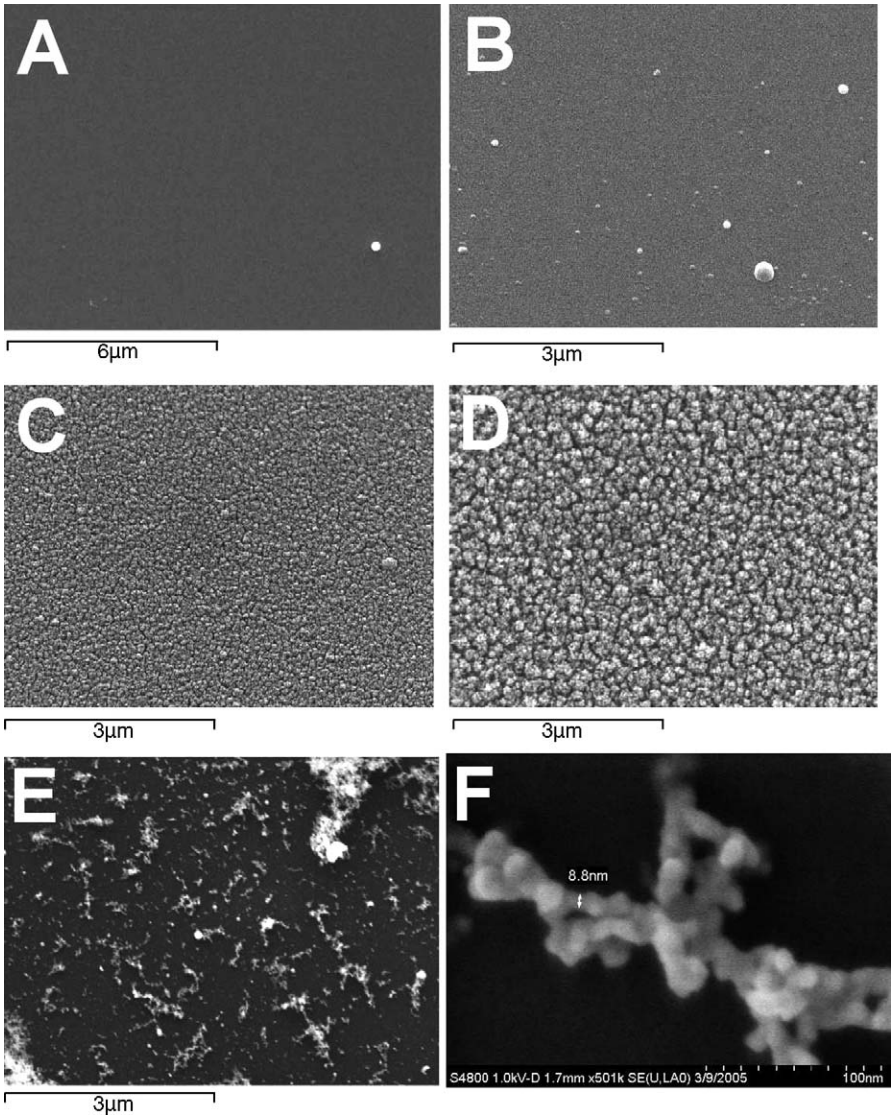

Fig. 1. SEM micrographs of tungsten films deposited in Ar at (A) 1 Pa, (B) 20 Pa, (C) 40 Pa, (D) 60 Pa, (E) 400 Pa, and (F) high resolution SEM image of a snowflake structure deposited at 1000 Pa dry air.

3. Results and discussion

Films deposited in inert gases (He, Ar) show a wide range of morphologies as a function of the background gas pressure, as revealed by SEM observations. SEM micrographs of films deposited in argon are shown in Fig. 1. In particular, increasing gas pressure from high vacuum conditions (10^{-5} Pa) up to a few Pa, films appear compact with a smooth surface. At a few tens Pa the roughness increases and the morphology begins to show a nano and mesostructure evolving progressively towards an open and porous structure. Finally, for gas pressure exceeding a few hundreds Pa (up to 1000 Pa) the film surface appears spotted with soft and snowflake structures emerging from a compact, smooth background. These structures are made of small nanoparticles, about 5–20 nm in diameter, as revealed by high-resolution SEM images (see Fig. 1F).

The same general trend is observed when helium is used as the background gas. Yet, the pressure thresholds between the above discussed morphologies (namely smooth, nanostructured and snowflake structures) are affected by the inert gas mass. Shifting from Ar to He, gas mass is reduced by a factor of 10 (i.e. from 40 to 4 a.m.u.). As a result, films deposited in helium begin to show a nanostructured surface at 60 Pa while the same threshold for argon is around 20 Pa. Moreover at 400 Pa He the films show a porous, sponge-like but connected structure, not yet revealing the snowflake structures already observable at 200 Pa in Ar.

AFM measurements were performed to better investigate the details of film surface and the crossover between different morphologies. AFM images shown in Fig. 2 compare the crossover from a compact, smooth to a nanostructured surface for films deposited either in helium or in argon. Moving from 40 to 60 Pa helium the surface morphology changes drastically and the surface roughness increases by a factor of 10 (from 0.2 to 2 nm rms roughness). A similar, though not identical, change is observed in argon moving from 10 to 20 Pa, even though the rms surface roughness does not increase significantly (from 0.5 to 1 nm). The trend of surface roughness as a function of gas pressure, shown in Fig. 3, reveals an abrupt increase of the roughness beyond 20 Pa Ar and 70 Pa He. This corresponds to a change in the film formation mechanisms. Beyond 100 Pa He, and beyond a slightly lower Ar pressure, not reliable AFM images could be obtained, owing to the presence of soft structures with high peak-to-valley ratios.

The overall observed morphologies are the result of the variation of the film growth mechanisms. In vacuum extremely smooth surfaces grow mainly atom by atom apart from the presence of some droplets presumably due to hydrodynamic sputtering of the target (typical PLD drawback). In a background gas the length of the ablation plume (at least its visible, light emitting, component) reduces when increasing gas pressure or mass [22]. This plume confinement favors cluster formation and the kinetic energy of the particles in the plume is

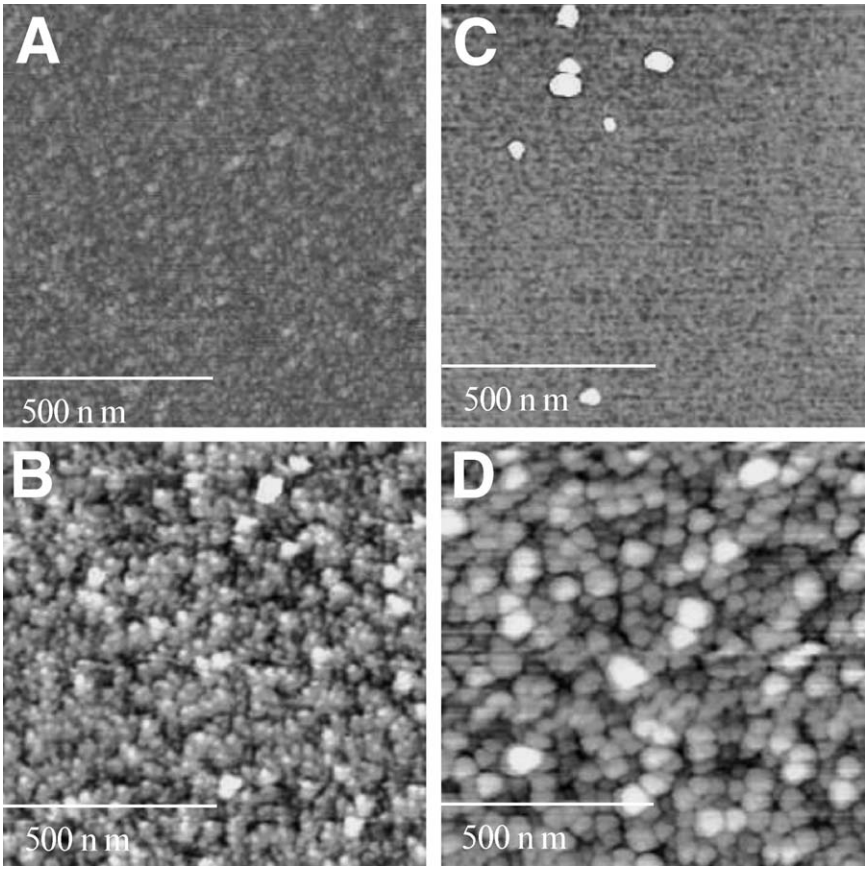

Fig. 2. 1 μm × 1 μm scan size AFM images of films deposited in He and Ar showing the pressure threshold between compact and nanostructured morphology. (A) 10 Pa-Ar, (B) 20 Pa-Ar, (C) 40 Pa-He, and (D) 60 Pa-He.

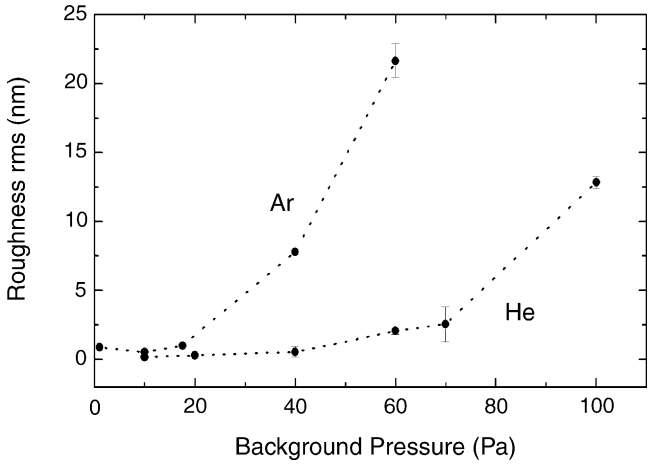

Fig. 3. Surface roughness of films deposited in He and Ar as a function of the gas pressure.

strongly reduced, especially when the plume becomes smaller than the target-to-substrate distance and particles diffuse in the background gas. In our experiments this transition occurs at about 30–40 Pa Ar and 100 Pa He and corresponds to the formation of highly porous nanostructured films with a marked three-dimensional growth. In this initial work the target-to-substrate distance and the energy density per pulse were kept constant, while pressure only was varied. The coupled effect of changing both gas pressure and target-to-substrate distance is currently under investigation.

Films were also deposited in dry air to study the capability of growing tungsten oxide films with controlled stoichiometry, crystallinity and morphology, starting from oxidized precursors. The surface morphology of these films is again characterized by the same general trend between different morphologies, with slightly smaller threshold pressures than for films deposited in argon. In this case a direct correlation between film morphology and gas mass is more difficult due to the chemical effect of oxygen on the ablated species. Raman spectra in Fig. 4 show the effect of depositing in an oxidizing atmosphere: at 10 Pa dry air the typical signal of amorphous tungsten oxide [23] starts to grow (broad bands at 100–500 and 600–1000 cm^{-1}), while at 1 Pa the absence of Raman signal suggests a metallic nature of the film. At about 40 Pa and at higher pressures the sharpening of the Raman bands towards well defined peaks indicates an increase of the correlation lengths maybe due to the presence of nanocrystals of increasing size. In particular, the low frequency features are related to O–W–O bending modes and to vibrations of WO_6 octahedral units; features in the 600–800 cm^{-1} range are related to W–O stretching modes [24], while the feature at about 960 cm^{-1} (whose intensity decreases and ultimately disappears with increasing pressure) has been attributed by some authors to W=O stretching modes at grain boundaries, observable when the grain size is in the nm range [25,26]. Finally, films deposited at 1000 Pa dry air show Raman peaks at 807, 718 and 270 cm^{-1}, typical of polycrystalline WO_3 in either monoclinic (γ) or triclinic (δ) phase (unique assignment is not possible due to the presence of these peaks in both the monoclinic and triclinic oxide phases). The presence of other weak features (such as the signals at roughly 640 and 678 cm^{-1}) suggests the coexistence of different oxide phases.

It is worth noticing that also Raman spectra of films deposited in inert gases reveal the tendency towards spontaneous oxidation when the samples are exposed to ambient air. Raman spectra as a function of the background inert gas pressure are shown in Fig. 5. Films deposited at low pressure are metallic (i.e. no Raman signal) while, increasing

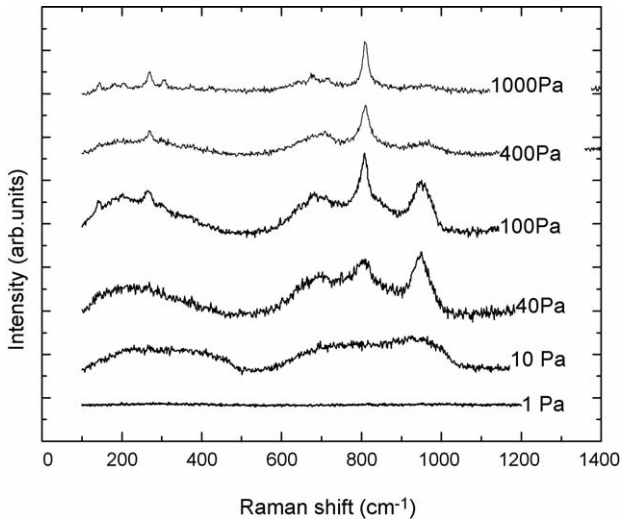

Fig. 4. Raman spectra of films deposited in dry air as a function of the gas pressure.

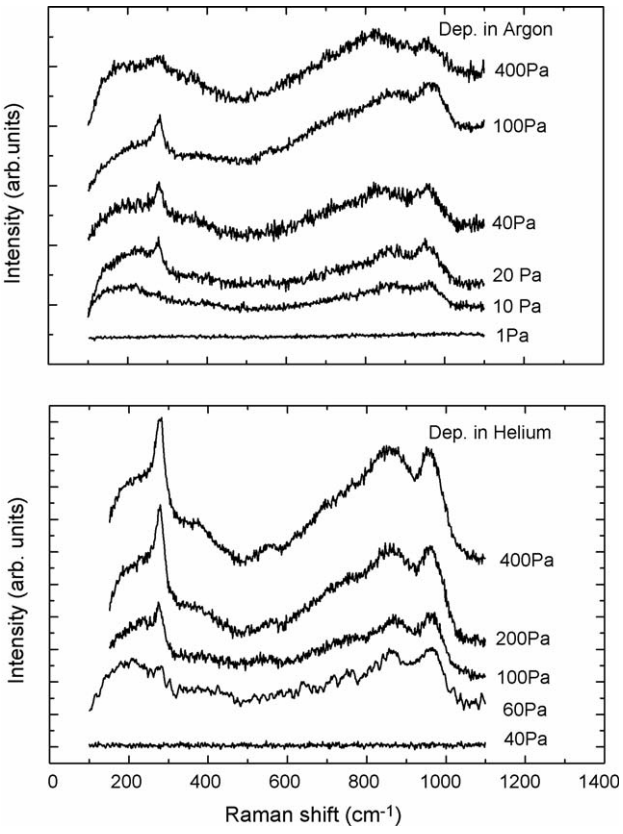

Fig. 5. Raman spectra of films deposited in Ar (top) and in He (bottom) as a function of gas pressure.

pressure, amorphous tungsten oxide bands start to grow. At higher pressures these bands do not evolve towards crystalline peaks (the 960 cm^{-1} peak is always present), apart from a peak at about 275 cm^{-1} which is anomalous in sharpness and intensity with respect to the rest of the spectrum, making it difficult a precise assignment (an assignment to WO_2 crystallites is not straightforward since the Raman spectrum of this phase is characterized by two strong peaks at 285 and 781 cm^{-1} with similar intensity [27]). From the spectra shown in Fig. 5 it is clear that the transition from metallic to amorphous oxide films takes place over the same pressure range where film morphology begins to change from compact to nanostructured, i.e. about 60 Pa for helium and 10–20 Pa for argon. In this case it is reasonable that a mainly surface oxidation occurs; the latter is favored by the nanostructuring of the building blocks and by the corresponding increase of the effective surface area of the deposited material. The spectra of the amorphous oxide phase observed in He and Ar depositions display some differences with respect to the amorphous WO_3 films deposited at low dry air pressures, i.e. the 275 cm^{-1} peak evolution and the position of the W–O stretching band. Further investigation is needed to understand the origin of these features and thus of the oxidation mechanisms. Of course, both in situ and spontaneous post-deposition oxidation take place when dry air is employed, and more experiments (e.g. in situ Raman scattering) are needed for a complete comprehension of the oxidation mechanisms.

4. Conclusions

In conclusion, tuning background gas mass and pressure as well as oxygen content in the PLD deposition chamber opens the possibility to grow nanostructured tungsten and tungsten oxide films with different degrees of oxidation and crystallinity, controlling the structure over several length scales. In particular, large specific surfaces can be obtained, making these materials interesting not only for sensing applications but also for other chemical application like catalysis.

In order to improve the control on the grown morphologies, current and future works are focused on the investigation of the influence of target-to-substrate distance and pulse energy density on plasma dynamics and aggregation and deposition mechanisms, and thus on film properties. Preliminary experiments indicate that the ability to control the above discussed film properties by tuning the pulsed laser deposition conditions can be easily extended to a wide variety of metal and metal oxide films.

Acknowledgements

The authors would like to thank Hitachi and Dr. Roland Schmidt for high resolution SEM images.

References

[1] A.M. Dhote, S.B. Ogale, Appl. Phys. Lett. 64 (21) (1994) 2809.
[2] G.M. Mikhailov, A.V. Chernykh, V.T. Petrashov, J. Appl. Phys. 80 (2) (1996) 948.
[3] R. Solarska, B.D. Alexander, J. Augustynski, J. Solid State Electrochem. 8 (2004) 748.
[4] P.R. Bueno, F.M. Pontes, E.R. Leite, L.O.S. Bulhoes, P.S. Pizani, P.N. Lisboa-Filho, W.H. Schreiner, J. Appl. Phys. 94 (2004) 2102.
[5] L. Meda, R.C. Breitkopf, T.E. Haas, R.U. Kirss, Thin Solid Films 402 (2002) 126.
[6] J.L. Solis, S. Saukko, L. Kish, C.G. Granqvist, V. Lantto, Thin Solid Films 391 (2001) 255.
[7] E.J. McLeod, V.I. Birss, Electrochim. Acta 51 (2005) 684–693.
[8] S. Jayaraman, T.F. Jaramillo, S.-H. Baeck, E.W. McFarland, J. Phys. Chem. B 109 (2005) 22958–22966.
[9] X.-L. Yang, et al. J. Mol. Catal. A: Chem. 241 (2005) 205–214.
[10] G. Murali Dhar, B.N. Srinivas, M.S. Rana, M. Kumar, S.K. Maity, Catal. Today 86 (2003) 45–60.
[11] Kusmiyati, N.A.S. Amin, Catal. Lett. 102 (2005) 69–78.
[12] M.G. Falco, S.A. Canavese, N.S. Fîgoli, Catal. Today 107–108 (2005) 778–784.
[13] D.B. Chrisey, G. Hubler, Pulsed Laser Deposition of Thin Films, Wiley & Sons, New York, 1994.
[14] P.R. Willmott, J.R. Huber, Rev. Mod. Phys. 72 (2000) 315.
[15] M.S. Tillack, D.W. Blair, S.S. Harilal, Nanotechnology 15 (2004) 390.
[16] D.H. Lowndes, et al. J. Mater. Res. 14 (1999) 359.
[17] D.B. Geohegan, A.A. Puretzky, G. Duscher, S.J. Pennycook, Appl. Phys. Lett. 72 (1998) 2987.
[18] R. Dolbec, E. Irissou, M. Chaker, D. Guay, F. Rosei, M.A. El Khakhani, Phys. Rev. B 70 (2004) 201406–201411.
[19] Zs. Marton, L. Landstrom, M. Boman, P. Heszler, Mater. Sci. Eng. C 23 (2003) 225.
[20] E. Salje, K. Viswanathan, Acta Cryst. A 31 (1975) 356.
[21] H. Kawasaki, J. Namba, K. Iwatsuji, Y. Suda, K. Wada, K. Ebihara, T. Ohshima, Appl. Surf. Sci. 197–198 (2002) 547.
[22] X.Y. Chen, S.B. Xiong, Z.S. Sha, Z.G. Liu, Appl. Surf. Sci. 115 (1997) 279.
[23] M. Boulova, G. Lucazeau, J. Solid State Chem. 167 (2002) 423.
[24] E. Salje, Acta Cryst. A 31 (1975) 360.
[25] M. Boulova, A. Gaskov, G. Lucazeau, Sens. Actuator B 81 (2001) 99.
[26] E. Cazzanelli, L. Papalino, A. Pennisi, F. Simone, Electrochim. Acta 46 (2001) 1937.
[27] G.L. Frey, et al. J. Solid State Chem. 162 (2001) 300–314.